JOURNAL OF GEOPHYSICAL RESEARCH, VOL. 102, NO. D12, PAGES 13,685–13,700, JUNE 27, 1997

Impact of sulfate aerosols on albedo and lifetime of clouds: A sensitivity study with the ECHAM4 GCM

Ulrike Lohmann[1] and Johann Feichter

Max Planck Institute for Meteorology, Hamburg, Germany

Abstract. A coupled sulfur chemistry-cloud microphysics scheme (COUPL) is used to study the impact of sulfate aerosols on cloud lifetime and albedo. The cloud microphysics scheme includes precipitation formation, which depends on the cloud droplet number concentration (CDNC) and on the liquid water content. On the basis of different observational data sets, CDNC is proportional to the sulfate aerosol mass, which is calculated by the model. Cloud cover is a function of relative humidity only. Additional sensitivity experiments with another cloud cover parameterization (COUPL-CC), which also depends on cloud water, and with a different autoconversion rate of cloud droplets (COUPL-CC-Aut) are conducted to investigate the range of the indirect effect due to uncertainties in cloud physics. For each experiment, two simulations, one using present-day and one using preindustrial sulfur emissions are carried out. The increase in liquid water path, cloud cover, and shortwave cloud forcing due to anthropogenic sulfur emissions depends crucially upon the parameterization of cloud cover and autoconversion of cloud droplets. In COUPL the liquid water path increases by 17% and cloud cover increases by 1% because of anthropogenic sulfur emissions, yielding an increase in shortwave cloud forcing of -1.4 W m^{-2}. In COUPL-CC the liquid water path increases by 32%, cloud cover increases by 3% and thus shortwave cloud forcing increases by -4.8 W m^{-2}. This large effect is caused by the strong dependence of cloud cover on cloud water and of the autoconversion rate on CDNC, cloud water, and cloud cover. Choosing a different autoconversion rate (COUPL-CC-Aut) with a reduced dependence on CDNC and cloud water results in an increase of liquid water path by only 11% and of cloud cover by 1%, and the increase in shortwave cloud forcing amounts to -2.2 W m^{-2}. These results clearly show that the uncertainties linked to the indirect aerosol effect are higher than was previously suggested.

1. Introduction

Aerosols may influence the Earth's radiation budget in two ways. First, they scatter solar radiation back to space, thus enhancing the planetary albedo. This effect is called the direct aerosol effect. The direct effect of anthropogenic sulfate aerosols has been estimated by different calculations, including climate model simulations, to range between -0.3 and -0.9 W m^{-2} [e.g., *Charlson et al.,* 1992; *Kiehl and Briegleb,* 1993; *Feichter et al.,* 1997]. Second, aerosols can act as cloud condensation nuclei (CCN). The number of available CCN is one of the parameters that determines the cloud droplet number concentration (CDNC), cloud albedo, and precipitation formation in warm clouds [*Albrecht,* 1989; *Fouquart and Isaka,* 1992]. As solar radiation is mainly scattered but hardly absorbed by cloud droplets and as an increase in CCN, for a constant liquid water content, leads to a larger concentration of cloud droplets of smaller radius, cloud reflectivity will be enhanced, so that the forcing is negative. This is one aspect of indirect aerosol forcing [*Twomey,* 1974; *Twomey et al.,* 1984]. It is by far more uncertain than the direct effect because the microphysical processes involved are not well understood [*Penner et al.,* 1994; *Intergovernmental Panel on Climate Change,* 1996].

Another aspect of the indirect effect [*Fouquart and Isaka,* 1992; *Hudson,* 1993] is the impact of changes of cloud droplet size on precipitation formation and residence time of clouds. The smaller the droplets, the less efficient the precipitation formation per cloud droplet. Therefore the residence time of clouds with small droplets is larger. *Parungo et al.* [1994] show that the increase of altocumulus and altostratus cloud amount observed over the period from 1952 to 1981 appears to be in accord with the geographic distribution of SO_2 emissions.

Observational evidence for the indirect aerosol effect has been reported from ship track observations [e.g., *Radke et al.,* 1989; *King et al.,* 1993], which reveal a simultaneous decrease in cloud droplet radii and increase in cloud albedo. During the Atlantic Stratocumulus Transition Experiment (ASTEX), *Garrett and Hobbs* [1995] and *Hudson and Li* [1995] found that a polluted cloud has a higher concentration of small droplets and almost no drizzle size droplets in comparison with a clean cloud. Numerical studies of marine stratocumuli support a feedback between lifetime and microphysical properties of clouds with prolonged cloud lifetime in clouds with smaller droplet radii. Additionally, by decreasing the precipitation efficiency, and consequently the aerosol removal rate, high CCN concentrations tend to be self-perpetuating [*Ackerman et al.,* 1995].

[1]Now at Canadian Centre for Climate Modeling and Analysis, Victoria, British Columbia, Canada.

Paper number 97JD00631.
0148-0227/97/97JD-00631$09.00

The indirect aerosol effect has been studied by using general circulation models by *Jones et al.* [1994], *Boucher and Lohmann* [1995], *Jones and Slingo* [1996], *Kogan et al.* [1996], *Chuang et al.* [1997], and *Feichter et al.* [1997]. All studies empirically relate CDNC to the mass of sulfate aerosols, assuming that the dominant source of CCN is sulfate aerosols. Most of them use monthly mean sulfate fields from the MOGUNTIA chemical transport model as input fields [*Langner and Rodhe,* 1991]. The studies differ in the empirical relationships used between sulfate aerosols and CDNC and the cloud optical properties. *Feichter et al.* [1997] apply the same empirical relationship as do *Boucher and Lohmann* but take the on-line simulated sulfate aerosol mass as an input field. The simulated indirect aerosol effect in those studies ranges between -0.5 W m^{-2} and -1.6 W m^{-2}. *Boucher and Lohmann* [1995] and *Jones and Slingo* [1996] estimate an uncertainty of the indirect aerosol forcing due to the assumed empirical relationship between -0.5 W m^{-2} and -1.5 W m^{-2} or between -0.5 W m^{-2} and -1.6 W m^{-2}, respectively. All studies estimate the change in cloud albedo by calculating the shortwave forcing with and without anthropogenic sulfur emissions (i.e., the meteorology remains unchanged assuming that the liquid water content of clouds has not changed between preindustrial and present-day conditions). Thus feedbacks on cloud microphysics are omitted.

Boucher and Rodhe [1994], on the other hand, assume that the precipitation formation rate depends on liquid water content and CDNC [*Boucher et al.,* 1995]. They perform two separate experiments: one with present-day sulfur emissions and one with preindustrial sulfur emissions. An increase in sulfate particles causes an increase in CDNC and thus a decrease in precipitation efficiency, prolonging cloud lifetime. As the input fields are monthly mean values of sulfate aerosol mass obtained from MOGUNTIA, there is no feedback on the removal of sulfate aerosols by clouds. The estimated indirect aerosol forcing ranges between -0.7 and -1.4 W m^{-2}.

In this paper we fully couple a sulfur cycle module [*Feichter et al.,* 1996] to the cloud microphysics scheme [*Lohmann and Roeckner,* 1996], so that aerosol-induced changes in the cloud microphysics can feed back on the sulfur cycle. Three pairs of experiments, each pair using preindustrial and present-day sulfur emissions, are performed to obtain the effect of sulfate aerosols on cloud lifetime and cloud albedo. The experiments differ in their parameterization of cloud cover and autoconversion rate, both of which are critical to the determination of the residence time of clouds. To estimate the indirect forcing due to changes in cloud albedo only, we rerun the present-day experiment and calculate diagnostically the shortwave radiative forcing from the monthly mean sulfate fields of the present-day experiment and the preindustrial one.

The ECHAM4 general circulation model, the new cloud microphysics scheme used in this study, and the sulfur cycle module are explained in section 2. A model validation of this coupled integration in terms of sulfate surface concentrations, liquid water path, and shortwave cloud forcing is given in section 3. In section 4 the indirect aerosol effect is discussed with respect to changes in cloud lifetime and to changes in cloud albedo. Discussion and conclusions are given in section 5.

2. Experiments and Model Description

The results presented below are based on three pairs of 5-year integrations at T30 resolution, each pair using present-day and preindustrial sulfur emissions. All of the experiments were integrated over the years 1985-1989 where the data from the Earth Radiation Budget Experiment (ERBE) with which we validate the model are available. The model is forced by observed sea surface temperatures and sea ice extents taken from the Atmospheric Model Intercomparison Project (AMIP) data set [*Gates,* 1992].

The first set of experiments uses the standard cloud scheme COUPL (see Table 1 and section 2.2). The second set uses the cloud cover parameterization of *Xu and Randall* [1996] (COUPL-CC), and the third set uses *Berry's* [1967] autoconversion rate and the cloud cover parameterization of *Xu and Randall* [1996] (COUPL-CC-Aut). The COUPL present-day experiment was rerun, calculating diagnostically the shortwave radiative forcing with the monthly mean sulfate aerosol concentrations from the present-day and preindustrial experiment of COUPL, respectively (COUPL-Albedo). For comparison between the present-day climate of COUPL and an uncoupled version, we used a 5-year integration of the standard ECHAM4 model [*Roeckner et al.,* 1996] (STAND).

2.1. Meteorological Model

The dynamics and part of the model physics of the ECHAM model have been adopted from the European Centre for Medium-Range Weather Forecasts (ECMWF) model [*Roeckner et al.,* 1996]. Prognostic variables are vorticity, divergence, temperature, (logarithm of) surface pressure, and the mass mixing ratios of water vapor and total cloud water (liquid and ice together). The model equations are solved on 19 vertical levels in a hybrid p-σ-system by using the spectral transform method with triangular truncation at wavenumber 30 (T30). Nonlinear terms and physical processes are evaluated at grid points of a "Gaussian grid" providing a nominal resolution of 3.75° times 3.75°. A semi-implicit leapfrog time integration scheme with Δt=30 min is used for the simulation with T30 resolution. Cumulus clouds are represented by a bulk model including the effects of entrainment and detrainment on the updraft and downdraft convective mass fluxes [*Tiedtke,* 1989]. An adjustment closure based on the convective available potential energy (CAPE) is used [*Nordeng,* 1994]. Organized entrainment is assumed to depend on buoyancy, and the parameterization of organized detrainment is based upon a cloud population hypothesis. The turbulent transfer of momentum, heat, water vapor, and total cloud water is calculated on the basis of a higher-order closure scheme [*Brinkop and Roeckner,* 1995]. The radiation code is based on a two-stream solution of the radiative transfer equation with six spectral intervals in the terrestrial infrared spectrum [*Morcrette,* 1991] and two in the solar part of the spectrum [*Fouquart and Bonnel,* 1980]. Gaseous absorption due to water vapor, CO_2, O_3, CH_4, N_2O, and CFCs is included, as well as scattering and absorption due to prescribed aerosols and model-generated clouds. The cloud optical properties are described in section 2.3. A new global set of land surface parameters, including surface background albedo, surface roughness length, leaf area index, fractional vegetation cover, and forest ratio [*Claussen et al.,* 1994], is used.

2.2. Cloud Microphysics Scheme

The cloud microphysics scheme used in the experiment COUPL is described in detail by *Lohmann and Roeckner* [1996]. Its main characteristic is the separate treatment of

Table 1. List of Experiments

Cloud Scheme	Present-Day (PD) Sulfur Emissions	Preindustrial (PI) Sulfur Emissions
Standard cloud scheme	STAND-PD	STAND-PI
Coupled sulfur cycle-cloud microphysics scheme COUPL (equations (1)-(4)	COUPL-PD	COUPL-PI
COUPL using *Xu and Randall's* [1996] cloud cover parameterization (equations (1)-(3), (5)-(6))	COUPL-CC-PD	COUPL-CC-PI
COUPL using *Xu and Randall's* [1996] cloud cover parameterization and *Berry's* [1967] autoconversion rate (equations (2)-(3), (5)-(7))	COUPL-CC-Aut-PD	COUPL-CC-Aut-PI
COUPL-PI rerun calculating the change in SCF by using the monthly mean sulfate aerosol distributions from COUPL-PD and COUPL-PI	COUPL-Albedo	COUPL-Albedo

cloud water and cloud ice as prognostic variables. In this scheme the bulk microphysics parameterizations for warm phase processes are based mainly on the model of *Beheng* [1994], while the parameterizations of the mixed and ice phase have been developed originally for a mesoscale model [*Levkov et al.*, 1992]. Parameterized microphysical processes are condensational growth of cloud droplets, depositional growth of ice crystals, homogeneous, heterogeneous, and contact freezing of cloud droplets, autoconversion of cloud droplets, aggregation of ice crystals, accretion of cloud ice and cloud droplets by snow and of cloud droplets by rain, evaporation of cloud water and rain, sublimation of cloud ice and snow, and melting of cloud ice and snow. The advection of cloud water and cloud ice is omitted. A parameterization of the autoconversion rate of cloud droplets [*Beheng*, 1994], which depends not only on the liquid water content but also on CDNC, is represented by (in SI units)

$$Q_{aut} = \frac{\left(\gamma_1 6 \cdot 10^{28} n^{-1.7} (10^{-6}\mathrm{CDNC})^{-3.3} \left(10^{-3} \rho \frac{q_l}{b}\right)^{4.7}\right)}{\rho} \quad (1)$$

where n (=10) is the width parameter of the initial cloud droplet spectrum, described by a Γ-function, ρ is the air density, γ_1 (=220) is a tunable parameter, q_l is the cloud water mixing ratio, and b is the fractional cloud cover. At present, CDNC cannot be computed realistically in GCMs, because it depends on several factors that are not easy to predict, such as subgrid-scale vertical velocity, maximum supersaturation, and availability of CCN. Therefore we empirically relate CDNC to the sulfate aerosol mass (SO_4^{2-}) [*Boucher and Lohmann*, 1995]. Measurements of SO_4^{2-}, CCN, and CDNC have been taken at various continental and marine sites in clean and polluted air, for a variety of weather situations. Hence empirical relationships between CDNC (per cubic meter) and SO_4^{2-} (in micrograms per cubic meter) can be derived for marine and continental clouds:

$$\mathrm{CDNC}_{mar} = 10^6 \cdot 10^{2.06 + 0.48 \log(SO_4^{2-})} \quad (2)$$

$$\mathrm{CDNC}_{cont} = 10^6 \cdot 10^{2.24 + 0.26 \log(SO_4^{2-})} \quad (3)$$

In *Lohmann and Roeckner* [1996] monthly mean values of SO_4^{2-} obtained from a sulfur cycle simulation with ECHAM4 [*Feichter et al.*, 1996] were used to calculate CDNC. In this study, CDNC is obtained from the sulfate aerosol concentrations calculated on-line (see section 2.4).

Fractional cloud cover, b, is an empirical function of the relative humidity [*Sundqvist et al.*, 1989]:

$$b = 1 - \sqrt{1 - b_o} \quad (4)$$

where $b_o=(r-r_0)/(1-r_0)$, r is the grid-mean relative humidity, and r_0 is a condensation threshold specified as a function of height following *Xu and Krueger* [1991].

Next, experiments were performed in which the parameterization of cloud cover follows an approach of *Xu and Randall* [1996] (COUPL-CC). It is based on observations during GATE and ASTEX. In contrast to the approach in COUPL, this parameterization depends not only on relative humidity but also on the cloud water content (q_w) (sum of liquid and ice):

$$b = r^{0.25}[1 - exp(-\beta q_w)] \quad (5)$$

where

$$\beta = 250[(1-r)q_{vs}]^{-0.45} \quad (6)$$

and q_{vs} is the saturation specific humidity. If the relative humidity exceeds 99.9% in a grid, a 100% cloud amount is assumed. For the formation of marine stratocumulus clouds below an inversion we apply the relative humidity approach used in ECHAM4.

Finally, experiments were performed in which the parameterization of the autoconversion rate from *Berry* [1967] was taken instead of the one from *Beheng* [1994] and the cloud cover parameterization from *Xu and Randall* (COUPL-CC-Aut):

$$Q_{aut} = \frac{\gamma_2 10^3 \rho \left(\frac{q_l}{b}\right)^2}{120 + \frac{5.7 \cdot 10^{-6}\mathrm{CDNC}}{10^3 \rho \frac{q_l}{b}}} \quad (7)$$

where γ_2=0.35.

2.3. Cloud Radiative Properties

The radiative properties of water droplets and approximately "equivalent" ice crystals are derived from Mie theo-

ry, and the results are fitted to the spectral resolution of the radiation model and formulated in terms of cloud droplet and ice crystal effective radii [*Rockel et al.*, 1991]. For liquid clouds the mean volume cloud droplet radius (r_v) is calculated from the cloud water mixing ratio in the cloudy part of the grid box (q_l/b) and CDNC as defined in (2) and (3):

$$r_v = \sqrt[3]{\frac{3q_l\rho}{4\pi b\rho_l \mathrm{CDNC}}} \tag{8}$$

where ρ_l is the water density.

Simultaneous measurements of r_v and the effective radius of cloud droplets (r_e) suggest a linear regression between the two radii:

$$r_e = kr_v \tag{9}$$

with k=1.143 for continental clouds and k=1.077 for marine clouds [*Johnson*, 1993].

2.4. Sulfur Chemistry

The parameterization of the sulfur chemistry is described in detail by *Feichter et al.* [1996]. Transport, dry and wet deposition, and chemical transformations of the constituents are calculated on-line with the GCM. Prognostic variables are dimethyl sulfide (DMS) and sulfur dioxide (SO_2) as gases and sulfate as an aerosol. The transport of these species due to advection, vertical diffusion, and convection is treated in the same way as the transport of water vapor. Biogenic emissions from the oceans and from soils and plants are assumed to occur as DMS; emissions from volcanoes, from biomass burning, and from combustion of fossil fuel and from smelting are assumed to occur as SO_2 [*Feichter et al.*, 1996, 1997]. As shown in Table 2, present-day emissions amount globally to 96.3 Tg sulfur per year, 72% of which are due to anthropogenic activities.

Dry deposition of SO_2 and of SO_4^{2-} at the ground is assumed to be proportional to the mixing ratio in the lowest model level and to a prescribed deposition velocity, which is 0.6, 0.8, and 0.1 cm s^{-1} over land, water, and snow, respectively, for SO_2 and which is 0.2 cm s^{-1} for SO_4^{2-} [*Langner and Rodhe*, 1991]. Since the turbulent transport is already performed in the meteorological model and the lowest model level is only 60 m, the error, in relation to a more sophisticated scheme, may be small. However, a new more extensive dry deposition scheme (resistance approach) for deposition of ozone has been developed for ECHAM [*Ganzeveld and Lelieveld*, 1995] and will be applied for SO_2 and for sulfate in the future.

Removal of SO_2 and sulfate by precipitation is calculated explicitly in terms of the model's precipitation formation rate [*Feichter et al.*, 1996]. DMS as well as SO_2 in the gaseous phase are oxidized by reaction with hydroxyl (OH) during the day. Additionally, DMS reacts with nitrate radicals (NO_3) at night. We have assumed that the only end product of DMS oxidation is SO_2, while in reality, DMS can also be oxidized to methanesulfonic acid (MSA) (as well as other oxidation products for which the yield is small and very uncertain). The consequence of our assumption is that we may slightly overestimate SO_2 and sulfate concentrations in marine regions. Two studies of the global sulfur cycle consider the oxidation pathway to MSA and found that only about 5% of the DMS is transformed to sulfate [*Chin et al.*, 1996; *Pham et al.*, 1995].

Dissolution of SO_2 within cloud water is calculated according to Henry's law. In the aqueous phase we consider oxidation of SO_2 by hydrogen peroxide (H_2O_2) and ozone (O_3). Three-dimensional monthly mean oxidant concentrations are prescribed on the basis of calculations with ECHAM and a more comprehensive chemical model [*Roelofs and Lelieveld*, 1995]. The calculation of the reaction rates and the effective Henry's law constant for SO_2 requires assumptions about the cloud pH. Assuming that aqueous phase equilibria and electroneutrality are maintained, and introducing the simplification that [S(IV)] = [HSO^{3-}], which can be applied if the pH ranges between 3 and 5, [H^+] is approximated by assuming a molar ratio between sulfate and ammonium of 1 [*Dentener and Crutzen*, 1994]. The end product of the gaseous and aqueous oxidation of SO_2 is sulfate (SO_4^{2-}) (for a more detailed description, see *Feichter et al.* [1996]).

3. Results

3.1. Simulated Sulfur Cycle

The annual mean sulfate burden is shown in Figure 1. In all experiments with present-day sulfur emissions, maxima are associated with high sulfur emissions due to industrial activity in North America, Europe, and Southeast Asia. Secondary maxima in the southern hemisphere (SH) are due to biomass burning and smelting. The sulfate burden over SH oceanic regions is below 5 mg m^{-2}. High levels of sulfate aerosols are transported downwind of the industrial centers off the shores of the Asian and North American coasts. In all preindustrial cases the sulfate burden hardly exhibits any distinct features except a maximum over Central Africa caused by biomass burning. Maxima over Indonesia and Kamchatka are due to volcanic emissions.

Table 2. Global Sulfur Emissions in Teragrams Sulfur per Year

Sources	References	Present-day	Preindustrial
Marine biosphere DMS	*Bates et al.* [1987], *Feichter et al.* [1996]	18.10	18.10
Terrestrial biosphere DMS	*Spiro et al.* [1992]	0.90	0.90
Background volcanic activity SO_2	*Spiro et al.* [1992], *Graf et al.* [1997]	8.00	8.00
Biomass burning SO_2	*Hao et al.* [1990]	2.50	0.25
Fossil fuel use and smelting SO_2	*Benkovitz et al.* [1994]	66.80	0.00
Total		96.30	27.25

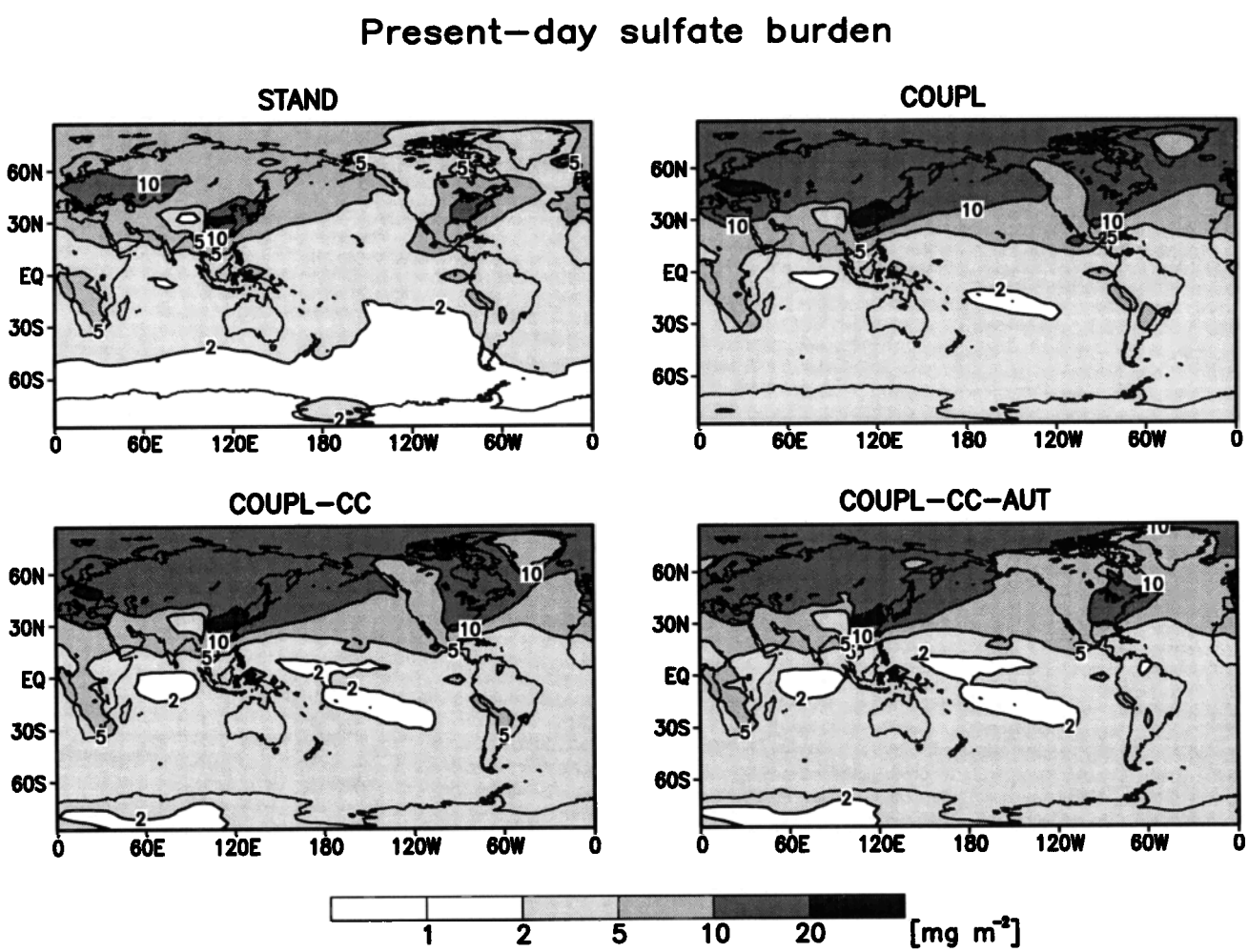

Figure 1. Annual mean sulfate burden for STAND, COUPL, COUPL-CC, and COUPL-CC-Aut for present-day emissions and preindustrial emissions. Contour spacing is 1, 2, 5, 10 and, 20 mg m^{-2}.

Table 3 compares the simulated sulfur cycle of the present-day COUPL experiment with the one calculated with the standard cloud scheme of ECHAM4 (STAND) [*Feichter et al.*, 1997] without any feedback between sulfate mixing ratios and cloud physics. The emissions and the chemical transformation rates are the same. In COUPL the sulfur dioxide (+23%) as well as the sulfate burden (+54%) is higher than that in STAND. In particular, high differences in the sulfate burden are found over the northern hemisphere (NH) in winter (+77%). Since the fraction of SO_2 that is oxidized to sulfate and the importance of the oxidation pathways is about the same in both experiments, these changes of the atmospheric load can be explained only by a longer atmospheric residence time of both species. The increase in the SO_2 burden may be attributed to the fact that the cloud physics parameterization used in COUPL produces lower cloud water mixing ratios in the lowest model levels. Since clouds are an effective sink for SO_2 (77% of SO_2 oxidation occurs in clouds), a longer travel time before an SO_2 particle enters a cloud results in a higher residence time and a higher burden. The higher sulfate burden also results from changes in the cloud scheme, especially from the interactions between the sulfur cycle and the cloud microphysics scheme. If the liquid water content remains constant, higher sulfate concentrations and, consequently, a higher number of cloud droplets reduces the likelihood of autoconversion of cloud droplets to rain drops and thus increases the residence time of cloud water. This effect, in turn, increases the atmospheric residence time of sulfate particles. The feedback process is terminated only by cloud evaporation. The importance of this feedback process is underlined by the fact that in the preindustrial low-emission scenario the differences in the sulfate burden between the operational and the new cloud microphysics experiments are much smaller (+20%) (Table 3).

Since only a few short-term airborne measurements of sulfate concentrations in the free troposphere are available, the simulated sulfate concentrations can be compared only with long-term surface observations. However, it is questionable whether the atmospheric burden can be evaluated solely on the basis of surface measurements. When we compare the surface mixing ratios of the operational and COUPL experiment over NH continents, where most of the observations are available, differences are much smaller for the surface concentrations than for the global burdens. Whereas the global burdens are higher in COUPL than in STAND by 23% and 54% for SO_2 and SO_4^{2-}, respectively, the NH continental surface concentrations are higher by only 4% for SO_2 and by 30% for SO_4^{2}. Hence it is difficult to verify the burden on the basis of

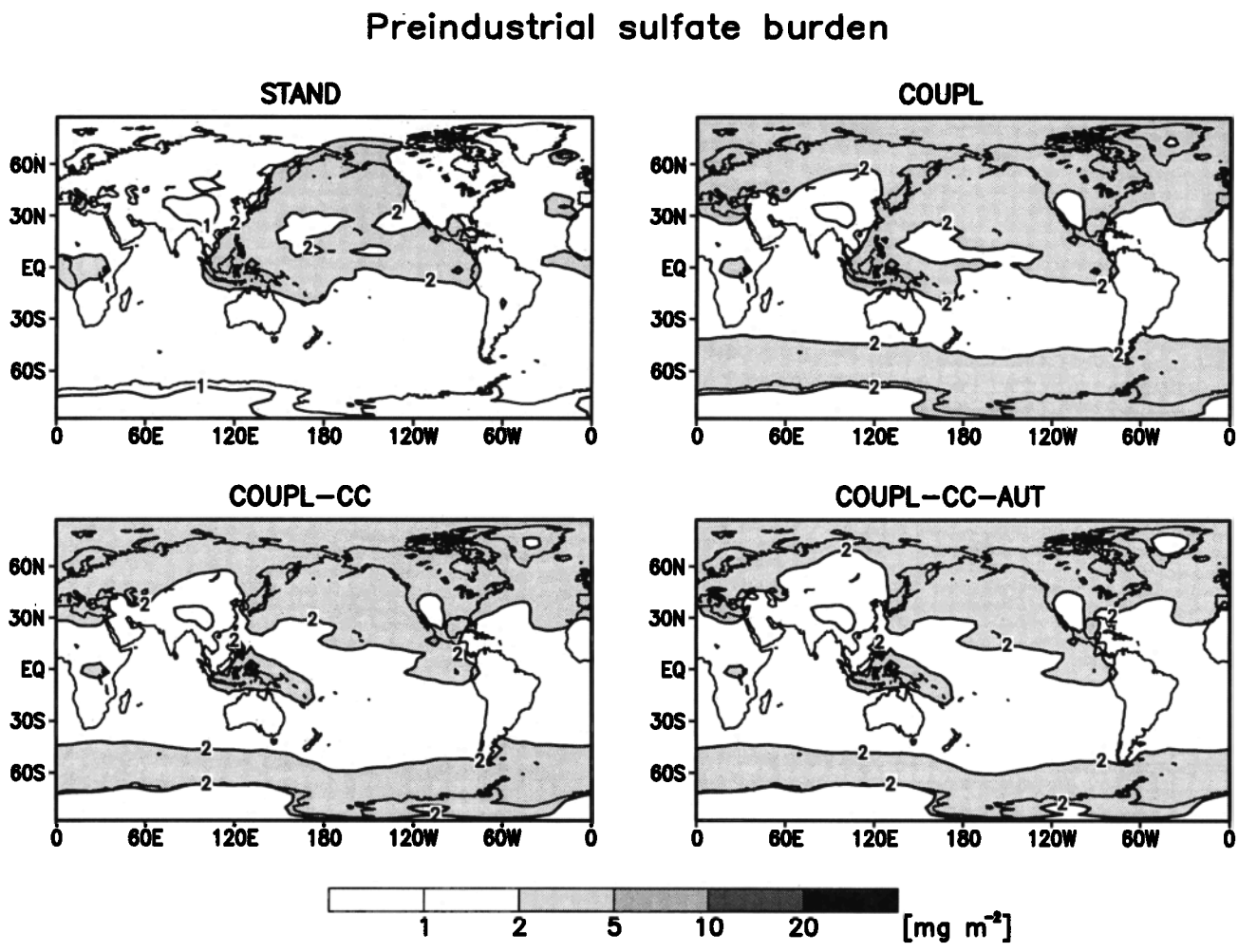

Figure 1. (continued)

surface observations, at least for SO_2. Figure 2 shows a comparison between the present-day experiments with the operational (STAND) as well as the new cloud physics coupled to the sulfur cycle (COUPL) and sulfate observations at various geographical locations observed over a period of at least 1 year [*Chin et al.*, 1996]. Arctic sites show a distinct maximum (Arctic haze) in late winter or spring that is underestimated by the model, in particular over the American Arctic. The simulated concentrations in winter over Europe are also too low, whereas the agreement with observations is quite good over the United States. Remote islands capture the seasonality quite well, but concentrations in Oahu are too high throughout the year. In contrast to the Arctic sites, the model agrees much better with observations in Antarctica. Differences between the model simulations are marked only in winter and spring with higher sulfate values in COUPL. These higher values slightly improve the agreement with observations, because in STAND the winter sulfate concentrations at high latitudes are underestimated [*Feichter et al.*, 1996].

The vertical distribution of sulfate is shown in Figure 3 for all present-day experiments. Maximum sulfate mixing ratios larger than 500 parts per trillion (ppt) occur in all experiments near the surface for the NH; the lowest values are found in the upper tropical troposphere. The most striking difference between STAND and the coupled experiments is the increase of the sulfate load in the coupled experiments in the extratropics. The region with sulfate mixing ratios higher than 500 ppt extends in COUPL and COUPL-CC from 30°N to the north pole, whereas in STAND such high values are only simulated between 30°N and 50°N.

3.2. Simulated Liquid Water Path and Shortwave Cloud Forcing

To understand the differences in the sulfate aerosol concentrations, the cloud water distribution of all present-day experiments is shown in Figure 4. All simulations show maxima in cloud water associated with shallow convection in the tropics and storm tracks in the extratropics. In COUPL, high values of cloud water near the surface are reduced in comparison with STAND, and cloud water at midlatitudes extends to higher levels. This feature is caused by the higher sulfate concentration, which yields higher values of CDNC and thus a reduction in autoconversion rate and an increase in residence time of water clouds. In turn, less sulfate is washed and rained out (see Figure 3). Therefore more sulfate aerosols can be transported toward the north pole and into higher levels. If Berry's autoconversion rate is used instead of Beheng's, the dependence of the autoconversion rate on CDNC and cloud water is reduced. Consequently, cloud water in COUPL-CC-Aut is lower mainly in regions with high sulfate in comparison with COUPL-CC. Thus sulfate aerosols are rained and washed out faster in COUPL-CC-Aut, so that the

Table 3. Global and Hemispheric Budgets and Sink Processes of SO_2 for STAND and COUPL for Preindustrial and Present-Day Emission Scenarios

	SO_2		SO_4^{2-}		Sinks of SO_2, %			
	Burden, Tg S	τ, days	Burden, Tg S	τ, days	Oxidation with OH	Oxidation with H_2O_2	Oxidation with O_3	Dry and Wet Deposition
				STAND				
Global annual mean								
Preindustrial	0.15	2.0	0.30	5.4	12	49	12	27
Present-day	0.44	1.6	0.68	4.4	12	41	5	42
NH January								
Preindustrial	0.11	3.0	0.13	4.7	10	44	21	25
Present-day	0.56	2.5	0.39	3.9	5	40	7	48
NH July								
Preindustrial	0.06	1.5	0.18	6.1	16	52	6	26
Present-day	0.23	1.2	0.56	5.0	22	35	1	42
				COUPL				
Global annual mean								
Preindustrial	0.18	2.4	0.36	6.2	12	57	8	23
Present-day	0.54	2.0	1.05	6.9	13	41	3	43
NH January								
Preindustrial	0.13	3.5	0.16	5.8	10	58	7	25
Present-day	0.73	3.2	0.69	6.6	6	37	3	54
NH July								
Preindustrial	0.07	1.7	0.19	6.2	14	53	9	24
Present-day	0 27	1.4	0.70	6.1	24	34	1	41

Oxidation plus deposition amounts to 100%. STAND results from *Feichter et al.* [1997].

area of sulfate concentrations of >500 ppt is much smaller in this model simulation.

Figure 5 presents the geographical distribution of the annual mean liquid water path (LWP) from all coupled experiments using present-day and preindustrial sulfur emissions, respectively, together with observations from special sensor microwave imager (SSM/I) data [*Greenwald et al.*, 1993; *Weng and Grody*, 1994]. The Greenwald et al. data set covers the period 1987-1991, and the Weng et al. data set covers 1987-1994. The accuracy of the retrieved LWP from microwave emissions over ice-free oceans is still rather low, and the retrievals can be affected by many input factors (e.g., total precipitable water, surface wind, and cloud temperature). There are also possible contributions from precipitation-size drops in the retrieved LWP. Hence the retrievals from Greenwald et al. and Weng and Grody differ regionally by a factor of 2 and in the global annual mean by 60%. We use both data sets as an estimate of the possible range of LWP.

COUPL-CC-PD and COUPL-PD are able to capture the observed maxima in LWP associated with tropical convection and NH extratropical cyclones, but they underpredict LWP over the SH oceans with respect to the retrieval of Greenwald et al. Because of high levels of sulfate aerosols (cf. Figure 1), and hence high concentration of cloud droplets, higher values of LWP than those observed are predicted over the western part of the North Atlantic and North Pacific in COUPL-PD and COUPL-CC-PD. Additionally, the convectively active regions in the tropics are more pronounced than those in the observations. In the experiment COUPL-CC-Aut-PD the overestimation of LWP off the shores of Asia and North America is reduced. Unfortunately, LWP associated with cyclone activity is reduced as well and lower than both observational data sets suggest. COUPL-CC-PI misses the maximum on NH oceans, which is pronounced in COUPL-CC-PD. For COUPL-CC-Aut the disagreement with observations is similar in the PD and PI sulfur emission scenarios. COUPL-PI, however, matches the observations no better or worse than COUPL-PD. To summarize, on the basis of the comparisons of the simulated LWP with observations it cannot be decided which approach is the better one and whether the consideration of anthropogenic sulfate aerosols improves the agreement with observations.

The differences in LWP between the present-day and preindustrial experiments give an idea of how sensitive the cloud scheme is to changes in CDNC. In the COUPL experiments, LWP increases globally by 17% from PI to PD, in COUPL-CC it increases by 32%, and in COUPL-CC-Aut in increases by 11% (cf. Table 4). The largest differences occur

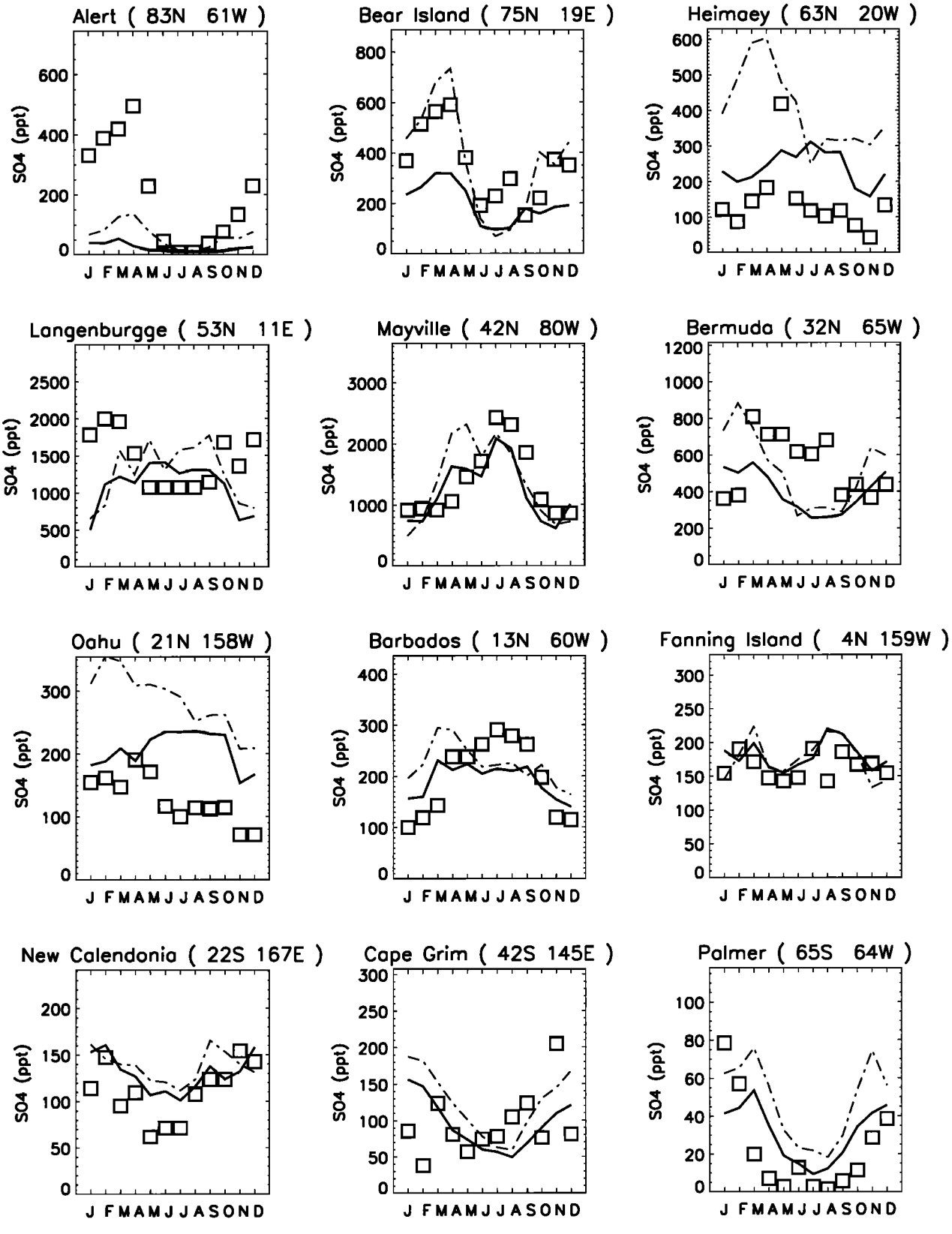

Figure 2. Surface sulfate concentrations as a function of time at different locations for observations [*Chin et al.*, 1996] (squares), STAND (solid line) and COUPL (dashed line).

over the NH oceans off the coast of industrial regions where the largest changes in SO_4^{2-} occur. Hardly any changes occur in the intertropical convergence zone (ITCZ) and in the SH, where sulfate aerosols are of natural origin except for sulfate aerosols from biomass burning.

The change in LWP between the PI and PD experiments is twice as large in COUPL-CC than in COUPL. As the sulfate distribution is similar in COUPL and COUPL-CC, the differences can be explained by the fact that the cloud cover depends only on relative humidity in COUPL but on both

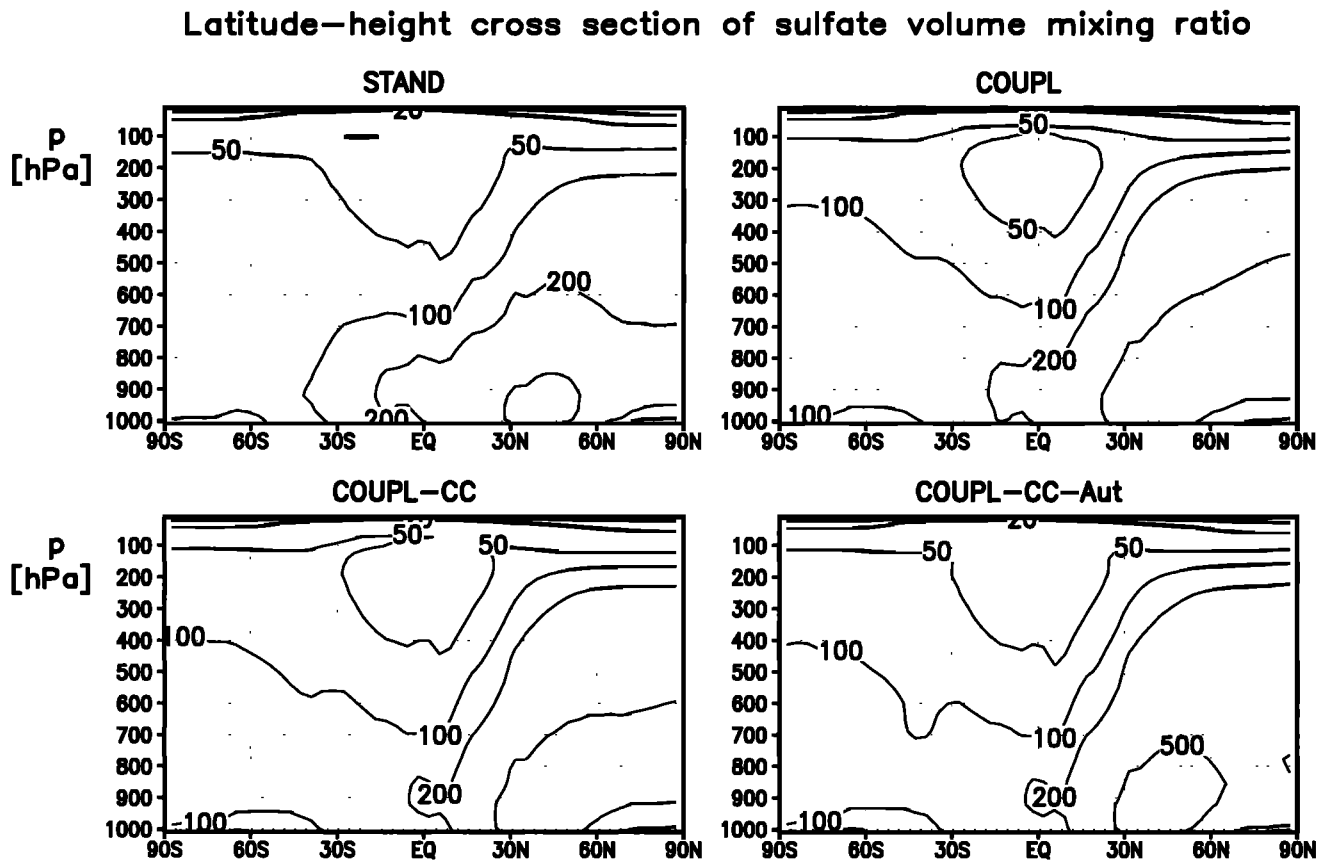

Figure 3. Annual mean latitude-height cross sections of sulfate volume mixing ratio for STAND, COUPL, COUPL-CC, and COUPL-CC-Aut for present-day emissions. Contour spacing is 10, 20, 50, 100, 200, 500, and 1000 ppt.

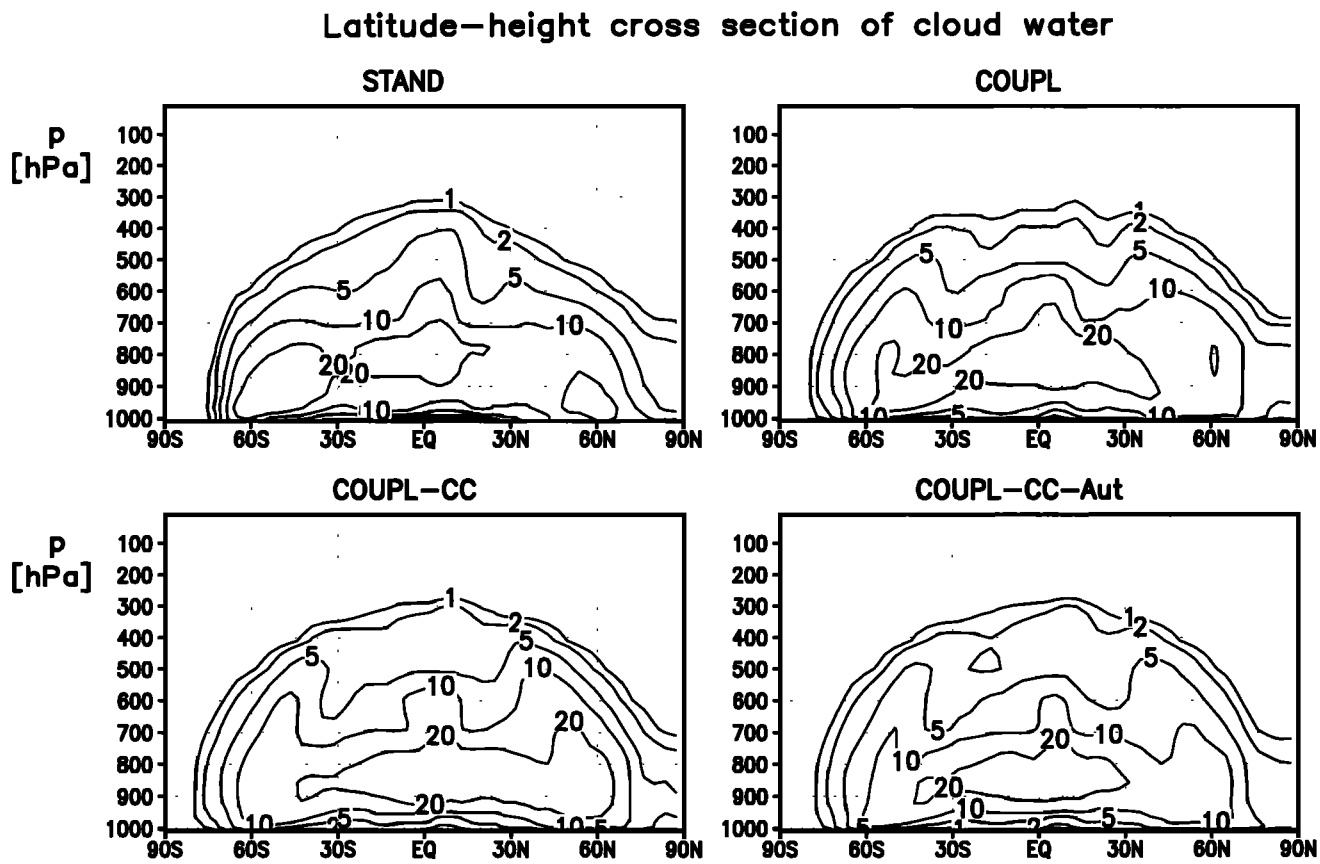

Figure 4. Annual mean latitude-height cross sections of cloud water for STAND, COUPL, COUPL-CC, and COUPL-CC-Aut for present-day emissions. Contour spacing is 1, 2, 5, 10, 20, and 50 mg kg^{-1}.

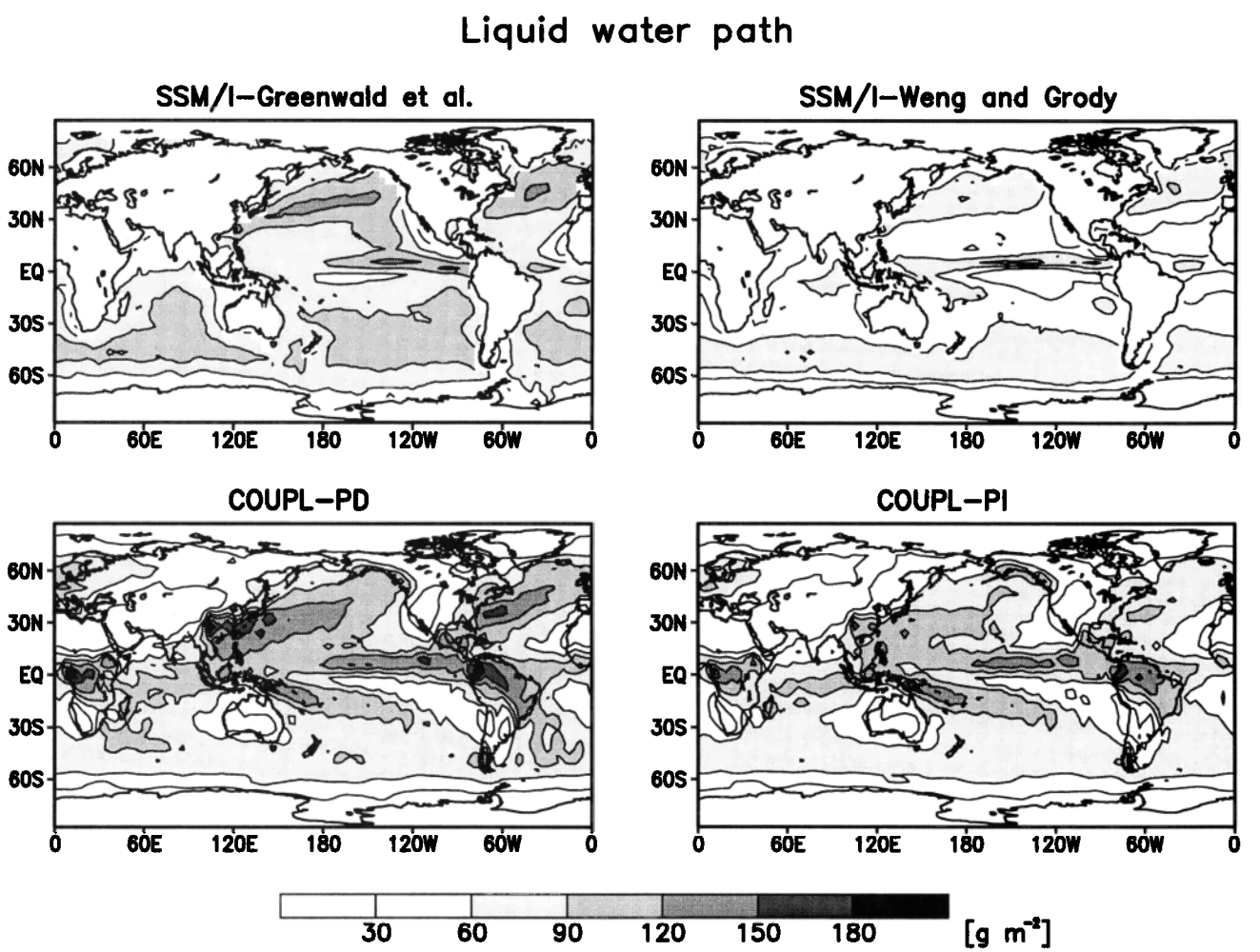

Figure 5. Geographical distribution of the annual mean liquid water path obtained from SSM/I analyses according to *Greenwald et al.* [1993] and *Weng and Grody* [1994] for COUPL-PD, COUPL-PI, COUPL-CC-PD, COUPL-CC-PI, COUPL-CC-Aut-PD, and COUPL-CC-Aut-PI. Contour spacing is 30 g m^{-2}.

relative humidity and cloud water in COUPL-CC. There a reduction in sulfur emissions reduces LWP, and consequently total cloud cover, more than is found in COUPL (3% in COUPL-CC in the global mean in comparison with 1% in COUPL). The autoconversion rate depends inversely on cloud cover, so that the reduced cloud cover, yields a faster autoconversion of cloud droplets, and again, LWP is reduced. This effect is not so pronounced in COUPL-CC-Aut, because Berry's autoconversion rate depends less strongly on CDNC, cloud water, and cloud cover than does Beheng's.

The influence of clouds on the shortwave radiation, SCF, is shown in Figure 6 for all coupled present-day experiments together with satellite observations from ERBE. Maxima in SCF in agreement with ERBE data occur where maxima in LWP are located (e.g., over tropical convectively active regions, NH storm tracks, and SH oceans). Secondary maxima are associated with marine stratocumulus decks off the coasts of California and South America. All simulations capture the overall features but underestimate SCF over SH oceans and NH storm tracks. In COUPL, SCF in the tropics is too high because of the overestimated LWP. In COUPL-CC and COUPL-CC-Aut, SCF in the ITCZ is not overestimated because of the lower LWP in the ITCZ. The magnitude of the secondary maxima associated with marine stratocumulus is too small in all experiments, because their total cloud cover is too low (not shown). Yet SCF is too high over oceanic subsidence regions in all experiments.

4. Indirect Aerosol Effect

Table 5 summarizes the global mean indirect aerosol effect, defined as the difference in shortwave cloud forcing between the PD and PI simulations for the three pairs of experiments, divided into hemispheric forcing and continental and oceanic forcing. The global mean indirect sulfate aerosol forcing is -1.4 W m^{-2} in COUPL, -4.8 W m^{-2} in COUPL-CC, and -2.2 W m^{-2} in COUPL-CC-Aut. Both experiments with Xu and Randall's cloud cover parameterization yield far larger indirect aerosol effects than those previously estimated. Even -1.4 W m^{-2} calculated with COUPL may be a high estimate of the indirect effect. This can be partly explained by the different experimental setups. In previous studies concerning the indirect aerosol effect, monthly mean sulfate aerosol concentrations from present-day and preindustrial sulfur emissions were used to calculate CDNC and thus the effective cloud droplet radius. Then the radiative forcing was calculated twice without changing the meteorology and, most important, without changing LWP or cloud lifetime. To compare our results with those studies, we also calculated the indirect effect in that manner, as the shortwave radiation dif-

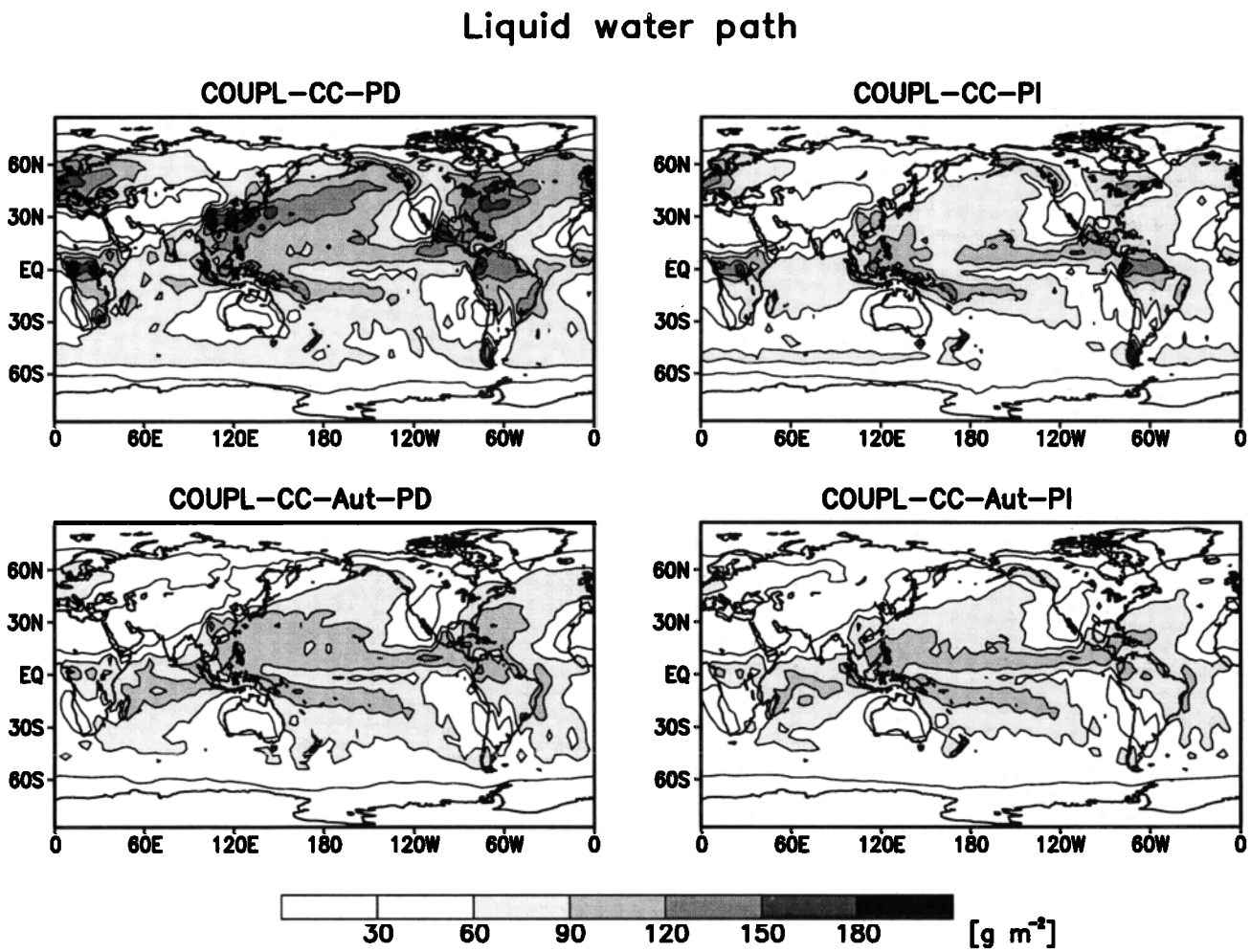

Figure 5. (continued)

Table 4. Globally Averaged Annual Mean Values of Water Vapor Mass, Liquid Water Path, Ice Water Path, Total Cloud Cover, Total Precipitation, Shortwave and Longwave Cloud Forcing and the Sulfate Burden of the Six Experiments

	WVM, kg m^{-2}	LWP, g m^{-2}	IWP, g m^{-2}	TCC, %	Precipitation, mm d^{-1}	SCF, W m^{-2}	LCF, W m^{-2}	SO_4^{2-}, Tg S
COUPL-PI	25.8	62.6	26.5	62.0	2.63	-46.7	29.8	0.36
COUPL-PD	25.8	73.3	26.4	62.5	2.61	-48.1	29.9	1.05
Diff (PD-PI)	...	10.7	-0.1	0.5	-0.02	-1.4	0.1	0.71
Percent	...	17.1	...	...	...	3.0	...	290.00
COUPL-CC-PI	24.9	55.3	25.8	58.3	2.54	-45.7	30.3	0.34
COUPL-CC-PD	24.8	72.9	25.9	59.9	2.52	-50.5	31.0	0.96
Diff (PD-PI)	-0.1	17.6	0.1	1.6	-0.02	-4.8	0.7	0.62
Percent	...	31.8	...	2.8	...	10.5	2.3	280.00
COUPL-CC-Aut-PI	25.0	51.6	25.7	57.8	2.58	-44.6	29.9	0.32
COUPL-CC-Aut-PD	25.1	57.3	25.6	58.4	2.55	-46.8	30.2	0.89
Diff (PD-PI)	0.1	4.7	-0.1	0.6	-0.03	-2.2	0.3	0.57
Percent	...	11.0	...	1.0	-1.16	4.9	1.0	280.00

Differences below 1% are not indicated. See text for definitions.

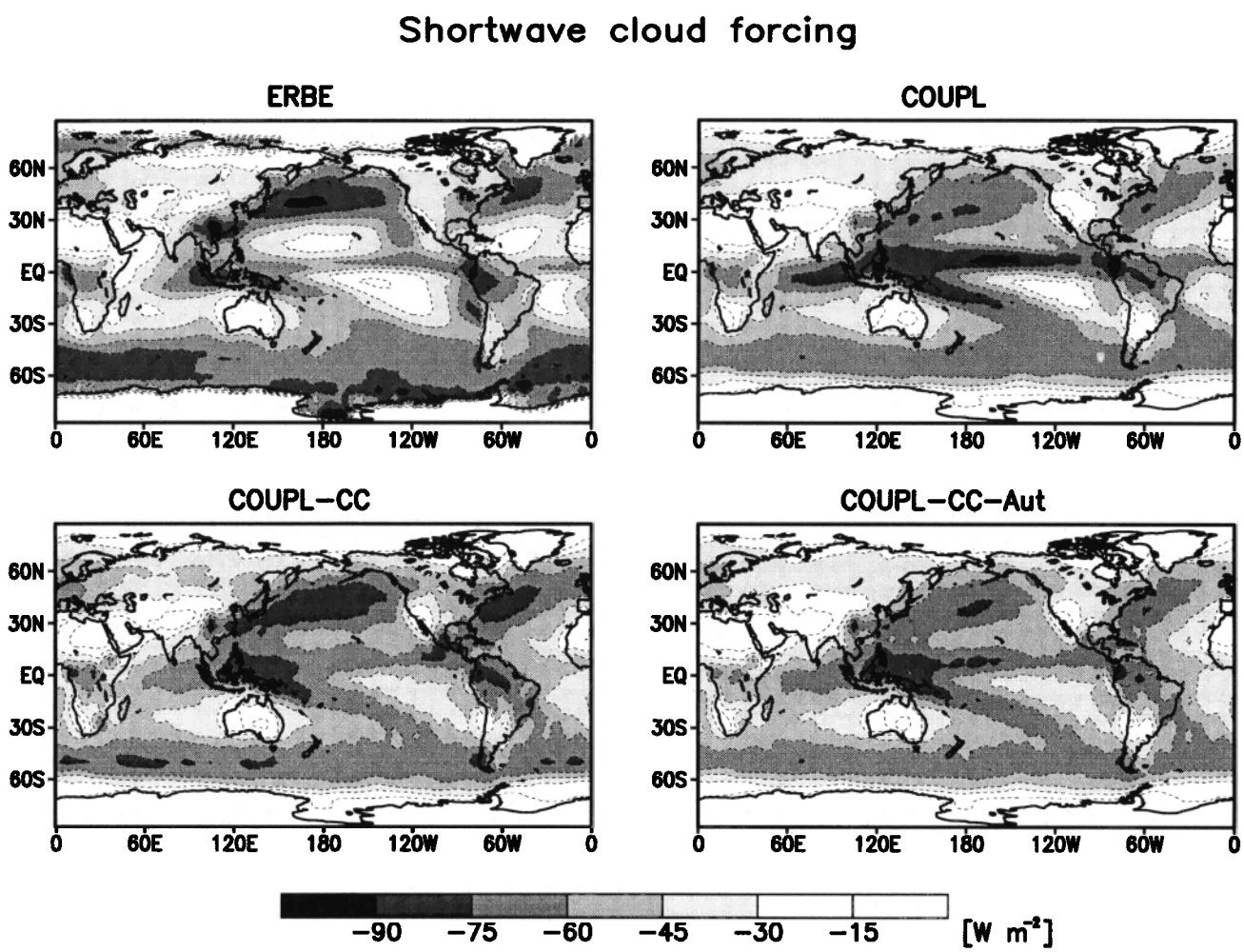

Figure 6. Geographical distribution of the annual mean shortwave cloud forcing obtained from ERBE, COUPL, COUPL-CC, and COUPL-CC-Aut. Contour spacing is 15 W m^{-2}.

ference between the different values of CDNC calculated from the monthly mean sulfate concentrations of COUPL-PD and COUPL-PI, using the meteorology and liquid water content of COUPL-PD (COUPL-Albedo). The resulting change in cloud albedo is -1 W m^{-2}, 30% lower than the combined effect (changes in cloud lifetime and albedo). As *Feichter et al.* [1997] pointed out, the cloud albedo effect calculated from monthly mean sulfate concentrations is 20% higher than the effect calculated from interactive sulfate concentrations. Thus the indirect effect due to changes in cloud albedo alone from interactive sulfate concentrations would amount to -0.8 W m^{-2}, which agrees with the cloud albedo effect calculated with STAND [*Feichter et al.*, 1997].

In all of the model simulations the indirect aerosol effect in the NH is about twice as large as that in the SH and higher over the oceans than over the continents. An ocean-land contrast with a larger forcing over the ocean is expected, because the applied relationship between the sulfate aerosol mass and CDNC has a steeper slope over the oceans [*Boucher and Lohmann*, 1995]. The NH-SH difference reflects the fact that most of the anthropogenic sulfate emissions occur in the NH.

Figure 7 shows the zonal mean changes in SCF, LWP, and cloud cover. In COUPL the largest increase in LWP is not accompanied by changes in cloud cover, so that the change in SCF has no distinct maximum in the NH midlatitudes. In COUPL-CC the changes in SCF, LWP, and cloud cover are largest at 40°N. Here an increase in LWP of 47 g m^{-2} and an increase in cloud cover of 5.5% yield an increase in SCF of 13 W m^{-2}. In COUPL-CC-Aut, in which Berry's autoconversion rate is used, the increase in LWP is at most 15 g m^{-2} and 2.5% in cloud cover, so that SCF increases not more than 5 W m^{-2}. The indirect effect in COUPL-CC and COUPL-CC-Aut is at maximum at NH midlatitudes, whereas in COUPL the maximum indirect effect is at 5°N.

Figure 8 shows the geographical distribution of the indirect aerosol effect for the three pairs of model simulations and the indirect effect due to albedo changes only (COUPL-Albedo).

Table 5. Global Mean, Hemispheric Mean, and Means Over Ocean and Land of the Indirect Aerosol Effect

Indirect Forcing, W m^{-2}	Global Mean	NH	SH	Ocean	Land
COUPL	-1.4	-2.0	-0.8	-1.7	-0.7
COUPL-CC	-4.8	-6.5	-3.1	-5.4	-3.3
COUPL-CC-Aut	-2.2	-2.9	-1.5	-2.5	-1.5
COUPL-Albedo	-1.0	-1.3	-0.7	-1.2	-0.5

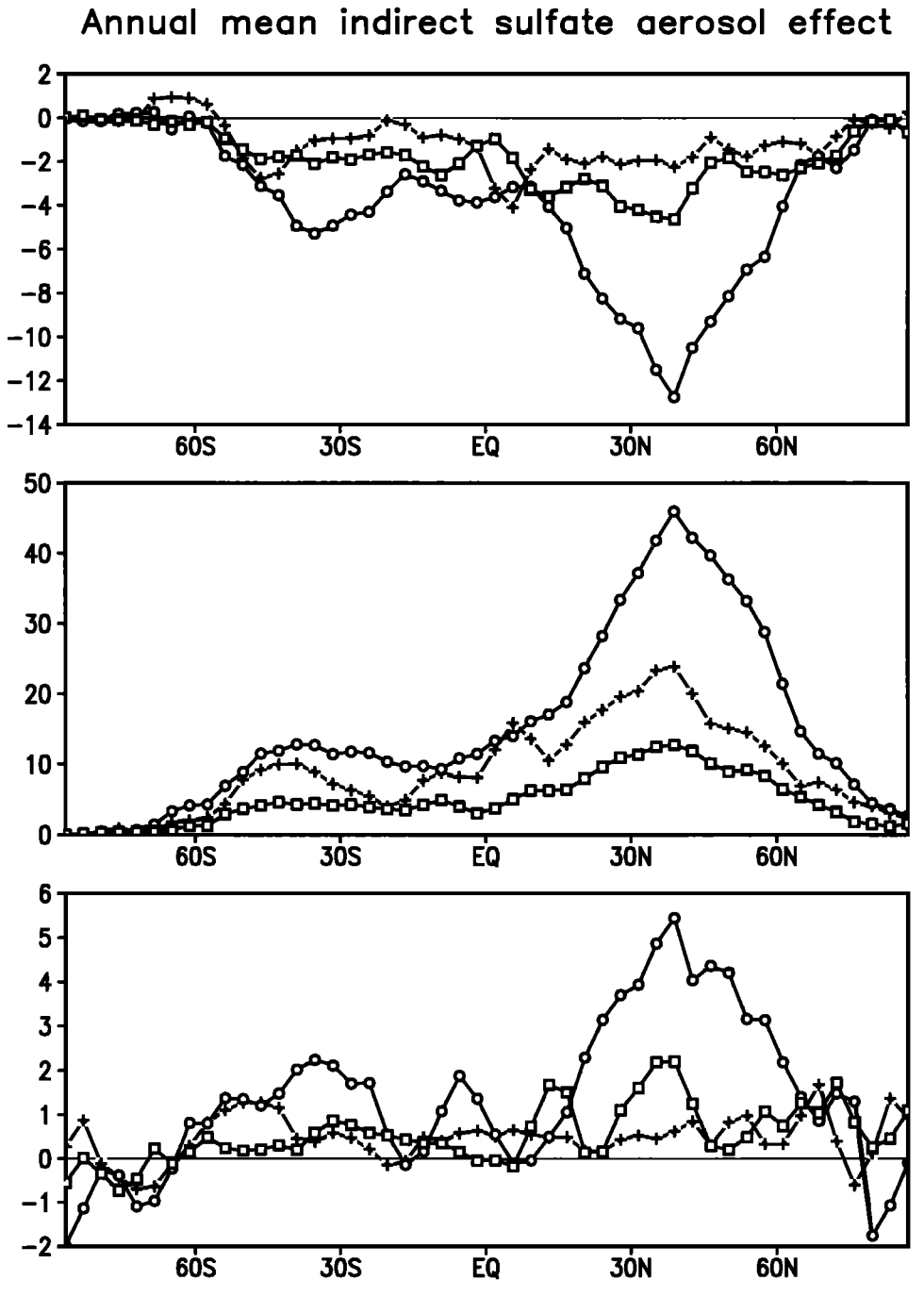

Figure 7. (top) Zonal and annual mean indirect sulfate aerosol forcing in W m^{-2} for COUPL (crosses), COUPL-CC (circles), and COUPL-CC-Aut (squares), (middle) change in LWP in g m^{-2}, and (bottom) change in cloud cover in percent.

The distribution of the indirect effect in COUPL-Albedo has maxima off the South American and African coasts but is mainly confined to the NH oceans similar to prior estimates by *Boucher and Lohmann* [1995] and *Feichter et al.* [1997]. All other distributions also show regions with decreasing SCF as a result of decreases in LWP and cloud cover. They are mainly confined to convectively active regions and SH oceans. Also, the indirect aerosol effect south of 30°S is larger than that in COUPL-Albedo. In COUPL a large indirect effect shows up off the African coast and over NH oceans where both cloud cover and LWP increase. The largest indirect effect, with maxima up to -20 W m^{-2} over NH oceans, is simulated with COUPL-CC. In COUPL-CC-Aut the distribution, as well as the magnitude of the indirect effect, is more similar to COUPL than to COUPL-CC.

In principle, the increase in cloud lifetime could affect the hydrological cycle. However, the total precipitation never decreases more than 1% between the present-day and preindustrial experiments, nor does the water vapor mass change significantly (Table 4). An increase in CDNC could lead to increased contact nucleation [*Baker,* 1997] and therefore more ice clouds. As the ice water path is almost the same in the

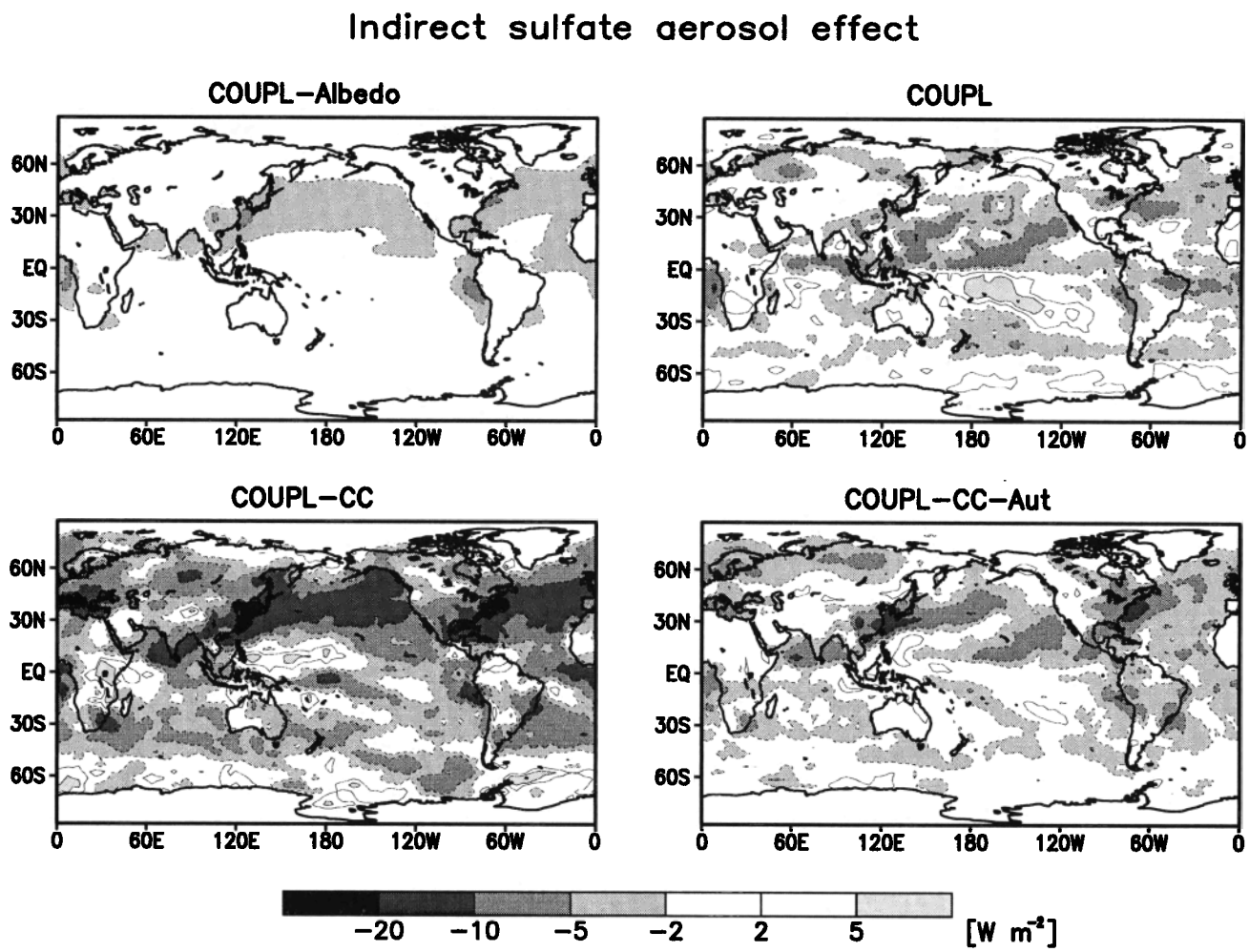

Figure 8. Annual mean indirect sulfate aerosol forcing for COUPL-Albedo, COUPL, COUPL-CC, and COUPL-CC-Aut. Contour spacing is -20, -10, -5, -2, 2, and 5 W m^{-2}.

preindustrial and present-day simulations, this impact is negligible. The change in longwave cloud forcing between the preindustrial and present-day experiments is also small in comparison with the change in shortwave cloud forcing.

5. Discussion and Conclusions

The indirect effect due to anthropogenic sulfate aerosols has been studied with a coupled microphysics-sulfate aerosol model (COUPL). This is the first time that the indirect aerosol effect due to a prolonging of cloud lifetime by changes in the precipitation efficiency and cloud albedo has been studied simultaneously with an interactive sulfur cycle module. To investigate the uncertainty in the indirect effect due to its dependence on cloud physics, sensitivity experiments with another cloud cover parameterization (COUPL-CC), and with another autoconversion rate of cloud droplets (COUPL-CC-Aut), have been conducted.

The findings of this study can be summarized as follows.

1. The sulfate burden is much higher in these coupled experiments than in STAND because of the longer residence time of water clouds.

2. The coupled model performs reasonably well, reproducing the main features of the observed surface sulfate concentrations, liquid water path, and shortwave cloud forcing.

3. In COUPL the indirect sulfate aerosol effect amounts to -1.4 W m^{-2}, approximately 60% of which is due to cloud albedo changes and 40% is due to changes in cloud lifetime. Thus consideration of the albedo effect only, as in all previous model simulations, underestimates the indirect forcing.

4. The largest indirect effect occurs over the NH oceans in all experiments. It is roughly twice as large in the NH as in the SH and twice as large over oceans as over land in all experiments.

5. The indirect effect of sulfate aerosols depends very much upon the parameterization of cloud cover and of the autoconversion rate of cloud droplets. Changes in the cloud cover parameterization lead to an increase in the indirect effect from -1.4 W m^{-2} in COUPL to -4.8 W m^{-2} in COUPL-CC. Simultaneously, the cloud cover and liquid water path increase rises from 1% and 17% in COUPL to 3% and 32% in COUPL-CC, respectively. An autoconversion rate where the dependence on CDNC and cloud water is weaker (COUPL-CC-Aut) results in a smaller indirect effect of -2.2 W m^{-2} and a change in cloud cover and liquid water path of only 1% and 11%, respectively.

A large uncertainty in our approach is the simple empirical relationship between CDNC and the sulfate aerosol mass (SO_4^{2-}), because other aerosols, such as nitrates and organic species, are locally at least as important as sulfate in acting as

CCN [*Hegg et al.*, 1993; *Novakov and Penner*, 1993; *Malm et al.*, 1994]. Sea salt aerosols can modify the pattern of the forcing because of their ability to nucleate earlier than sulfate aerosols. Although this effect may not change the global mean sulfate aerosol forcing, it may change the regional pattern [*Lowe et al.*, 1996]. Applying a relationship between SO_4^{2-} and CDNC further implies that SO_4^{2-} is a constant fraction of the total aerosol mass, which is definitely not what has been observed. The fraction of the total aerosol mass comprised by SO_4^{2-} ranges from 14% to 100% [*Hegg et al.*, 1993, 1995; *Malm et al.*, 1994; *Warneck*, 1988]. Even though *Hegg et al.* [1995] find that SO_4^{2-} makes up, on average, 62% of the total mass of accumulation mode particles, they conclude that in their limited data set most of the CCN were not sulfate. Also, the indirect effect depends upon the mixing approach. *Chuang et al.* [1997] simulated an indirect effect between -0.6 W m^{-2} and -1.2 W m^{-2} for internal mixing with aqueous conversion fractions of anthropogenic sulfate between 85% and 65% and -1.6 W m^{-2} for external mixing.

ECHAM4 does not account for cloud inhomogeneities. If sulfate aerosols change cloud inhomogeneities by changing secondary flows, this effect could have an impact on cloud albedo as well [*Baker*, 1997]. Also, a better representation of boundary layer clouds could change our results.

From the microphysical point of view, the cloud cover parameterization of Xu and Randall, used in COUPL-CC, has the advantage over that of Sundqvist et al., used in COUPL, in that it depends on cloud water as well as on the grid mean relative humidity. However, since the observations from which Xu and Randall's parameterization is derived do not include purely stratiform clouds, the cloud water dependence may not be generally valid. Of course, the indirect effect of -4.8 W m^{-2} obtained with this cloud cover parameterization (COUPL-CC) is as large as the forcing resulting from the doubling of CO_2, and it is very unlikely that the indirect sulfate aerosol effect is this large. Both autoconversion rates from Beheng and Berry used in COUPL-CC and COUPL-CC-Aut, respectively, are derived from the stochastical collection equation. Since autoconversion rates cannot be directly validated with observations, it is hard to judge which one is preferable. One can state only that it is perilous to use an autoconversion rate that depends as strongly on CDNC as Beheng's does in conjunction with a cloud cover parameterization that in turn depends on cloud water. Thus small changes in sulfur emissions, or in the relationship between the mass of sulfate aerosols and CDNC, will be amplified. We conclude that the uncertainties linked to the indirect aerosol effects on radiative forcing are much higher than was previously suggested.

Acknowledgments. This research was supported by grant EC Environment project SINDICATE. We thank Erich Roeckner, Lennart Bengtsson, and the anonymous reviewers for helpful comments and suggestions.

References

Ackerman, A. S., O. B. Toon, and P. V. Hobbs, Numerical modeling of ship tracks produced by injections of cloud condensation nuclei into marine stratiform clouds, *J. Geophys. Res., 100*, 7121-7133, 1995.

Albrecht, B. A., Aerosols, cloud microphysics, and fractional cloudiness, *Science, 245*, 1227-1230, 1989.

Baker, M., Cloud microphysics and climate, *Science*, in press, *1997*.

Bates, T. S., J. D. Cline, R. H. Gammon, and S. R. Kelly-Hansen, Regional and seasonal variations in the flux of oceanic dimethylsulfide to the atmsophere, *J. Geophys. Res.*, *92*, 2930-2938, 1987.

Beheng, K. D., A parameterization of warm cloud microphysical conversion processes, *Atmos. Res., 33*, 193-206, 1994.

Benkovitz, C. M., C. M. Berkowitz, R. C. Easter, S. Nemesure, R. Wagener, and S. E. Schwartz, Sulfate over the North Atlantic and adjacent continental regions: Evaluation for October and November 1986 using a three-dimensional model driven by observation-derived meteorology, *J. Geophys. Res.*, *99*, 20,725-20,756, 1994.

Berry, E. X., Cloud droplet growth by collection, *J. Atmos. Sci., 24*, 688-701, 1967.

Boucher, O., and U. Lohmann, The sulfate-CCN-cloud albedo effect: A sensitivity study with two general circulation models, *Tellus, 47 Ser. B*, 281-300, 1995.

Boucher, O., and H. Rodhe, The sulfate-CCN-cloud albedo effect: A sensitivity study, *Rep. CM-83*, 20 pp., Dep. of Meteorol., Stockholm Univ., Sweden, 1994.

Boucher, O., H. Le Treut, and M. B. Baker, Precipitation and radiation modelling in a GCM: Introduction of cloud microphysical processes, *J. Geophys. Res., 100*, 16,395-16,414, 1995.

Brinkop, S., and E. Roeckner, Sensitivity of a general circulation model to parameterizations of cloud-turbulence interactions in the atmospheric boundary layer, *Tellus, 47 Ser. A*, 197-220, 1995.

Charlson, R. J., S. E. Schwartz, J. M. Hales. R. D. Cess, J. A. Coagley Jr., J. E. Hansen, and D. J. Hofmann, Climate forcing by anthropogenic aerosols, *Science, 255*, 423-430, 1992.

Chin, M., D. J. Jacob, G. M. Gardner, M. Foreman-Fowler, and P. S. Spiro, A global three-dimensional model of tropospheric sulfate, *J. Geophys. Res., 101*, 18,691-18,700, 1996.

Chuang, C. C., J. E. Penner, K. E. Taylor, A. S. Grossman, and J. J. Walton, An assessment of the radiative effects of anthropogenic sulfate. *J. Geophys. Res., 102*, 3761-3778, 1997.

Claussen, M., U. Lohmann, E. Roeckner, and U. Schulzweida, A global data set of land-surface parameters, *Rep. 135*, 30 pp., Max-Planck-Inst. für Meteorol., Hamburg, Germany, 1994.

Dentener, F. J., and P. J. Crutzen, A three-dimensional model of the global ammonia cycle, *J. Atmos. Chem. 19*, 331-369, 1994.

Feichter, J., E. Kjellström, H. Rodhe, F. Dentener, J. Lelieveld, and G. J. Roelofs, Simulation of the tropospheric sulfur cycle in a global climate model, *Atmos. Environ., 30*, 1693-1707, 1996.

Feichter, J., U. Lohmann, and I. Schult, The atmospheric sulfur cycle and its impact on the shortwave radiation, *Clim. Dyn.*, in press, 1997.

Fouquart, Y., and B. Bonnel, Computations of solar heating of the Earth's atmosphere: A new parameterization, *Beitr. Phys. Atmos., 53*, 35-62, 1980.

Fouquart, Y., and H. Isaka, Sulfur emission, CCN, clouds and climate: A review, *Ann. Geophys. 10*, 462-471, 1992.

Ganzeveld, L. and J. Lelieveld, Dry deposition parameterization in a chemistry general circulation model and its influence on the distribution of reactive trace gases, *J. Geophys. Res., 100*, 20,999-21,012, 1995.

Garrett, T. J. and P. V. Hobbs, Long-range transport of continental aerosol over the Atlantic oceans and their effects on cloud structures, *J. Atmos. Sci., 52*, 2977-2984, 1995.

Gates, W. L., AMIP: The atmospheric model intercomparison project, *Bull. Am. Meteorol. Soc., 73*, 1962-1970, 1992.

Graf, H.-F., J. Feichter, and B. Langmann, Volcanic sulfur emissions: Estimates of source strength and its contribution to the global sulfate distribution, *J. Geophys. Res.*, in press, 1997.

Greenwald, T. J., G. L. Stephens, T. H. Vonder Haar, and D. L. Jackson, A physical retrieval of cloud liquid water over the glo-

bal oceans using special sensor microwave/imager (SSM/I) observations, *J. Geophys. Res., 98,* 18,471-18,488, 1993.

Hao, W. M., M. H. Liu, and P. J. Crutzen, Estimates of annual and regional releases of CO_2 and other trace gases to the atmosphere from fires in the tropics, pp. 440-462, Springer-Verlag, New York, 1990.

Hegg, D. A., R. J. Ferek, and P. V. Hobbs, Light scattering and cloud condensation nucleus activity of sulfate aerosol measurements over the northeast Atlantic Ocean, *J. Geophys. Res., 98,* 14,887-14,894, 1993.

Hegg, D. A., P. V. Hobbs, R. J. Ferek, and A. P. Waggoner, Measurements of some aerosol properties relevant to radiative forcing on the east coast of the United States, *J. Appl. Meteorol., 34,* 2306-2315, 1995.

Hudson, J. G., Cloud condensation nuclei. *J. Appl. Meteorol., 32,* 596-607, 1993.

Hudson, J. G., and H, Li, Microphysical contrasts in Atlantic stratus, *J. Atmos. Sci., 52,* 2031-3040, 1995.

Intergovernmental Panel on Climate Change, *Climate Change 1995: The science of climate change.*, Edited by J. T. Houghton et al., 572 pp., Cambridge Univ. Press, New York, 1996.

Johnson, D. W., Parameterisation of the cloud topped boundary layer: Aircraft measurements, in *Parameterization of the Cloud Topped Boundary Layer,* pp. 77-117, Eur. Cent. for Medium-Range Weather Forecasts, Reading, England, 1993.

Jones, A., and A. Slingo, Predicting cloud droplet effective radius and indirect sulphate aerosol forcing using a general circulation model, *Q. J. R. Meteorol. Soc., 122,* 1573-1595, 1996.

Jones, A., D. Roberts, and A. Slingo, A climate model study of the indirect radiative forcing by anthropogenic sulphate aerosols, *Nature, 370,* 450-453, 1994.

Kiehl J. T., and B. P. Briegleb, The relative roles of sulfate aerosols and greenhouse gases in climate forcing, *Science, 260,* 311-314, 1993.

King, M. D., L. F. Radke, and P. V. Hobbs, Optical properties of marine stratocumulus clouds modified by ships, *J. Geophys. Res., 98,* 2729-2739, 1993.

Kogan, Z. N., Y. L. Kogan, and D. K. Lilly, Study of the anthropogenic sulfate aerosols indirect effect in marine stratocumulus clouds. Paper presented at 12th International Conference on Clouds and Precipitation, International Commission on Clouds and Precipitation, Zurich, Switzerland, 1996.

Langner, J., and H. Rodhe, A global three-dimensional model of the global sulfur cycle, *J. Atmos. Chem., 13,* 225-263, 1991.

Levkov, L., B. Rockel, H. Kapitza, and E. Raschke, 3D mesoscale numerical studies of cirrus and stratus clouds by their time and space evolution, *Beitr. Phys. Atmos., 65,* 35-58, 1992.

Lohmann, U., and E. Roeckner, Design and performance of a new cloud microphysics scheme developed for the ECHAM general circulation model, *Clim. Dyn., 12,* 557-572, 1996.

Lowe, J. A., M. H. Smith, C. D. O'Dowd, and S. L. Clegg, The effect of sea-salt aerosol on the production of sulphate in the marine atmospheric boundary layer and its effect on stratiform clouds. Paper presented at 12th International Conference on Clouds and Precipitation, International Commission on Clouds and Precipitation, Zurich, Switzerland, 1996.

Malm, W. C., J. F. Sisler, D. Huffman, R. A. Eldred, and T. A. Cahill, Spatial and seasonal trends in particle concentration and optical extinction in the United States, *J. Geophys. Res., 99,* 1347-1370, 1994.

Morcrette, J. J., Radiation and cloud radiative properties in the European Centre for Medium Range Weather Forecasts forecasting system, *J. Geophys. Res, 96,* 9121-9132, 1991.

Nordeng, T. E., Extended versions of the convective parameterization scheme at ECMWF and their impact on the mean and transient activity of the model in the tropics. *Tech. Memo. 206,* 41 pp., Eur. Cent. for Medium-Range Weather Forecasts, Reading, England, 1994.

Novakov, T., and J. E. Penner, Large contribution of organic aerosols to cloud-condensation-nuclei concentrations, *Nature, 365,* 823-826, 1993.

Parungo, F., J. F. Boatman, H. Sievering, S. W. Wilkinson, and B. B. Hicks, Trends in global marine cloudiness and anthropogenic sulfur, *J. Clim., 7,* 434-440, 1994.

Penner, J. E., R. J. Charlson, J. M. Hales, N. S. Laulainen, R. Leifer, T. Novakov, J. Ogren, L. F. Radke, S. E. Schwartz, and L. Travis, Quantifying and minimizing uncertainties of climate forcing by anthropogenic aerosols, *Bull. Am. Meteorol. Soc., 75,* 375-399, 1994.

Pham, M., J.-F. M. Mullter, G. P. Brasseur, C. Granier and G. M. Megie, A three-dimensional study of the tropospheric sulfur cycle, *J. Geophys. Res. 100,* 26,061-26,092, 1995.

Radke, L. F., J. A. Coagley Jr., and M. D. King, Direct and remote sensing observations of the effects of ships on clouds, *Science, 246,* 1146-1149, 1989.

Rockel, B., E. Raschke, and B. Weyres, A parameterization of broad band radiative transfer properties of water, ice and mixed clouds, *Beitr. Phys. Atmos., 64,* 1-12, 1991.

Roeckner, E., K. Arpe, L. Bengtsson, M. Christoph, M. Claussen, L. Dümenil, M. Esch, M. Giorgetta, U. Schlese, and U. Schulzweida, The atmospheric general circulation model ECHAM4: Model description and simulation of the present-day climate. *Rep. 218,* 90 pp., Max-Planck-Inst. für Meteorol., Hamburg, Germany, 1996.

Roelofs, G.-J., and J. Lelieveld, Distribution and budget of O_3 in the troposphere calculated with a chemistry general circulation model, *J. Geophys. Res., 100,* 20,983-20,998, 1995.

Spiro, P. A., D. J. Jacob, and J. A. Logan, Global inventory of sulfur emissions with 1 deg. times 1 deg. resolution, *J. Geophys. Res., 97,* 6023-6036, 1992.

Sundqvist, H., E. Berge, and J. E. Kristjansson, Condensation and cloud parameterization studies with a mesoscale numerical weather prediction model, *Mon. Weather Rev., 117,* 1641-1657, 1989.

Tiedtke, M., A comprehensive mass flux scheme for cumulus parameterization in large-scale models, *Mon. Weather Rev., 117,* 1779-1800, 1989.

Twomey, S. A., Pollution and the planetary albedo, *Atmos. Environ. 8,* 1251-1256, 1974.

Twomey, S. A., M. Piepgrass, and T. L. Wolfe, An assessment of the impact of pollution on global cloud albedo, *Tellus 36 Ser. B,* 356-366, 1984.

Warneck, P., *Chemistry of the Natural Atmosphere.* Int. Geophys. Ser. Vol. 41, 757 pp., Academic, San Diego, Calif., 1988.

Weng, F., and N. C. Grody, Retrieval of cloud liquid water using the special sensor microwave imager (SSM/I), *J. Geophys., Res., 99,* 25,535-25,551, 1994.

Xu, K. M., and S. K. Krueger, Evaluation of cloudiness parameterizations using a cumulus ensemble model, *Mon. Weather Rev., 119,* 342-367, 1991.

Xu, K. M., and D. A. Randall, A semiempirical cloudiness parameterization for use in climate models, *J. Atmos. Sci., 53,* 3084-3102, 1996.

J. Feichter, Max-Planck-Institut für Meteorologie, Bundesstrasse 55, 20149 Hamburg, Germany. (e-mail: feichter@dkrz.de)

U. Lohmann, Canadian Centre for Climate Modelling and Analysis, Atmospheric Environment Service, University of Victoria, P.O. Box 1700, Victoria, British Columbia, Canada V8W 2Y2. (e-mail: ulrike.lohmann@ec.gc.ca)

(Received October 16, 1996; revised January 21, 1997; accepted January 23, 1997.)